
¹⁸F-FDG PET/CT in Erdheim–Chester Disease: Imaging Findings and Potential BRAF Mutation Biomarker

Jason R. Young¹, Geoffrey B. Johnson^{1,2}, Robert C. Murphy¹, Ronald S. Go³, and Stephen M. Broski¹

¹Department of Radiology, Mayo Clinic, Rochester, Minnesota; ²Department of Immunology, Mayo Clinic, Rochester, Minnesota; and ³Department of Hematology, Mayo Clinic, Rochester, Minnesota

The purpose of this study was to evaluate ¹⁸F-FDG PET/CT for the diagnosis, management, and treatment of Erdheim–Chester disease (ECD). **Methods:** Our institutional database (2007–2017) was retrospectively reviewed for patients with pathologically proven ECD. A chart review yielded demographics, clinical information, and 5 categories of clinical impact. Two radiologists in consensus interpreted the images. Imaging findings were correlated with clinical data. **Results:** Seventy-one ¹⁸F-FDG PET/CT examinations were performed for 32 patients. The average SUV_{max} of the most active disease site was 9.2 (SD, 6.1). The most common sites involved were the skeleton (90.6% of patients, including 47% with axial and pelvic skeletal involvement), kidneys (81.3%), and central nervous system (CNS) (46.9%). Twenty-six patients were tested for a proto-oncogene B-Raf^{V600E} (BRAF) mutation (18 had the mutation and 8 did not). The presence of a BRAF mutation was associated with ¹⁸F-FDG-avid CNS disease ($P = 0.0357$), higher SUV_{max} ($P = 0.0044$), and greater mortality ($P = 0.0215$). The presence of CNS disease had 88% specificity and a 92% positive predictive value for predicting the presence of a BRAF mutation. PET/CT examination results influenced patient management in 48% of cases (34/71). **Conclusion:** ¹⁸F-FDG PET/CT results may act as a biomarker for the presence of a BRAF mutation, aid in establishing a diagnosis, guide biopsies, and gauge the treatment response in ECD patients. Axial and pelvic skeletal involvement is greater than previously reported.

Key Words: Erdheim–Chester disease; BRAF; PET/CT; histiocytosis

J Nucl Med 2018; 59:774–779

DOI: 10.2967/jnumed.117.200741

Erdheim–Chester disease (ECD) is a systemic histiocytosis that can involve several organs, with severity ranging from occult to life-threatening. The disease was first described by William Chester in 1930 after working with Austrian pathologist Jakob Erdheim (1). Even today, a correct diagnosis of ECD often takes years, given the rarity and variable manifestations of ECD.

Historically, there have been 3 broad categories of histiocytosis: malignant, Langerhans cell histiocytosis (LCH), and non-Langerhans cell histiocytosis. A modern 5-group scheme classifies ECD with LCH into the “L group” (2). Histologically, ECD has xanthomatous features, fibrosis, and occasional Touton giant cells. ECD histiocytes

stain positive for CD68 and negative for CD1a, langerin, and S100 (rarely ECD can stain faintly positive for S100) (3).

Recently, the presence of a BRAF mutation in ECD patients was discovered (4). Some reports suggested that BRAF mutations are universally present in ECD, but most indicated about 50% involvement (2,5). BRAF mutations are associated with various malignancies, including pulmonary adenocarcinoma, melanoma, papillary thyroid and colorectal carcinomas (6–11). For this reason, ECD has been classified as a malignant disorder (12). The presence of a BRAF mutation narrows the diagnosis toward ECD and LCH, excluding all other types of histiocytosis (13). Treatment of ECD is also guided by BRAF status. Patients without a BRAF mutation (BRAF–) tend to have a moderately favorable response to cladribine (14), whereas patients with a BRAF mutation (BRAF+) respond well to targeted therapy with vemurafenib (15–21).

The diagnosis of ECD is on the rise, with at least 750 reported cases to date (22), but diagnosis is challenging given the rarity and varied presentation of ECD. Common symptoms include dyspnea, bone pain, ataxia, and visual disturbance (3). Although skeletal lesions are almost universally present on imaging, only 50% of patients have bone pain (23).

Imaging plays a key role in diagnosing ECD. The sine qua non finding in ECD has been lower-extremity diaphyseal long-bone osteosclerosis (24–27). The osseous findings are best identified using ^{99m}Tc-methylene diphosphonate scintigraphy (bone scan) and are often difficult to detect radiographically (28). Several other sites commonly involved include the central nervous system (CNS), orbits, lungs, cardiovascular system, and retroperitoneum (29–37). Radiography, CT, and MRI have been used for focused evaluation. However, morphologic imaging may not accurately depict the severity or extent of disease or the response to therapy. In contrast, ¹⁸F-FDG PET/CT has been shown to have value for the systemic evaluation and quantification of the severity of ECD (38–41)—yet the data are scant.

Here, we review the largest set of single-center ¹⁸F-FDG PET/CT examinations to date, in patients with pathologically confirmed ECD. The aims of this study were to retrospectively analyze the utility of ¹⁸F-FDG PET/CT for the diagnosis, management, and treatment of patients with ECD and to correlate disease patterns and ¹⁸F-FDG activity with clinical data, including patient demographics, presenting symptoms, mortality, laboratory, histologic, and genetic data.

MATERIALS AND METHODS

Patient Selection

An institutional review board–approved retrospective review of a single-center institutional database was performed; the need to obtain

Received Aug. 15, 2017; revision accepted Oct. 12, 2017.
For correspondence or reprints contact: Stephen M. Broski, Mayo Clinic, 200 First St., S.W., Rochester, MN 55901.
E-mail: broski.stephen@mayo.edu
Published online Nov. 2, 2017.
COPYRIGHT © 2018 by the Society of Nuclear Medicine and Molecular Imaging.

informed consent was waived. A list of patients who underwent ^{18}F -FDG PET/CT (from February 15, 2007, through February 21, 2017) was cross-referenced with the following terms: erdheim, chester, histiocytosis, fibrosis, and nonlangerhan. Subjects who met the following criteria were included: a clinical diagnosis of ECD, a tissue diagnosis (biopsy or surgical excision) consistent with ECD, an age of greater than 18 y, and no active coexisting malignancy.

Chart Review

The following information was recorded: age, race, sex, chief complaint, type of tissue for pathologic review, BRAF mutation status and test method, serum C-reactive protein level erythrocyte sedimentation rate (within 30 d of ^{18}F -FDG PET/CT), and treatment history. The impact of ^{18}F -FDG PET/CT on patient management was determined by a chart review 6 mo after ^{18}F -FDG PET/CT, with attention to clinical, surgical, imaging, and pathology reports. Five categories of impact were recorded: contributing to the initial diagnosis of ECD, directing a subsequent biopsy, supporting the initiation or escalation of therapy, supporting the deescalation of or a holiday from therapy, and supporting continuation of the current clinical strategy.

Imaging Protocol

All ^{18}F -FDG PET/CT examinations were performed with 3-dimensional detectors according to standard oncologic clinical protocols. All patients fasted for at least 6 h and had blood glucose levels of less than 200 mg/dL at the time of the examination. Images were acquired 60–70 min after the intravenous administration of 370–555 MBq (10–15 mCi) of ^{18}F -FDG. Patients were imaged with the arms up if possible, covering at least the orbits to the mid thighs (128×128 matrix, 3–5 min/bed position, depending on the body mass index). Low-dose CT was performed for attenuation correction and anatomic localization.

Imaging Review

MIM software (MIM Software Inc.) was used for image review. All examinations were reviewed in consensus by a nuclear radiology fellow and a board-certified nuclear radiologist (5 y of clinical experience). SUVs (SUV_{max}) were derived from body weight and volumes of interest, incorporating the most metabolically active disease. ^{18}F -FDG-avid disease was considered present if uptake was visually greater than that of normal adjacent structures or the blood pool, when appropriate. Sites of ^{18}F -FDG-avid disease were grouped into the CNS, orbital, paranasal sinus, pleural, cardiac/pericardiac, vascular, retroperitoneal, renal, skeletal, mesenteric/peritoneal, and gonadal; other, less common sites of disease were noted individually. For SUV analysis, including between-

group comparisons (BRAF+ vs. BRAF–), only examinations obtained without treatment in the preceding 6 mo were included. Contributory CT findings were also recorded. A subset of 13 patients who underwent ^{18}F -FDG PET/CT for both staging and restaging was evaluated using PET Response Criteria in Solid Tumors guidelines (42). The remaining studies could not be evaluated using these guidelines because of incomplete imaging data, treatment before initial examination, or delay between initial scan and therapy initiation.

Statistical Analysis

Data were analyzed using JMP software for Macintosh (JMP Pro, version 11.2.1; SAS Institute Inc.). Continuous variables were expressed as mean and SD. Categorical variables were expressed as absolute and relative frequencies. The *P* values for between-group comparisons of continuous data were calculated from a Kruskal–Wallis 1-way ANOVA. For categorical variables, *P* values were computed from contingency tables using the Fisher exact test. Statistical significance was established for *P* values of less than 0.05.

RESULTS

Patient Population and Demographics

Of the patients meeting the initial inclusion criteria, 2 were excluded because the clinical and pathologic presentation was mixed ECD and Rosai–Dorfman disease. Thirty-two patients (12 women and 20 men) were included; their mean age at the time of the first ^{18}F -FDG PET/CT examination was 60.1 y (range, 32–83 y), 91% (29/32) were white, 6% (2/32) were Asian, and race was not reported for 3% (1/32). Common comorbidities included renal failure (25% [8/32]) and diabetes insipidus (31% [10/32]). Mortality secondary to ECD at the time of data collection was 12.5% (4/32). The most common presenting symptoms were dyspnea (28% [9/32]), bone pain (19% [6/32]), and visual disturbance (12.5% [4/32]).

Twenty-six subjects were tested for a BRAF mutation; 18 had the mutation and 8 did not. The BRAF mutations were substitutions of valine for glutamate at codon 600 (V600E) in all patients but 1, who had a V471F mutation. Methods of BRAF mutation analysis included immunohistochemical staining (9 positive and 6 negative), polymerase chain reaction (2 positive and 2 negative), next-generation genomic profiling (2 positive and 1 negative), and urinary cell-free DNA (8 positive and 2 negative). Some patients underwent more than 1 type of test to confirm BRAF status.

Imaging Results

Seventy-one ^{18}F -FDG PET/CT examinations were performed for 32 patients over a 10-y period. The number of examinations showed an upward trend over time: 1 in 2007, 2 in 2008, 2 in 2009, none in 2010, 2 in 2011, 3 in 2012, 6 in 2013, 12 in 2014, 16 in 2015, 21 in 2016, and 6 in the first quarter of 2017. The average SUV_{max} of the single most ^{18}F -FDG-avid lesion among all patients was 9.2 (SD, 6.1; range, 2.0–34.0).

The skeletal system was most commonly involved (91% [29/32]), with an average SUV_{max} of 4.5 (range, 1.5–15.7). Most cases involved the appendicular long bones, particularly around the knees. However,

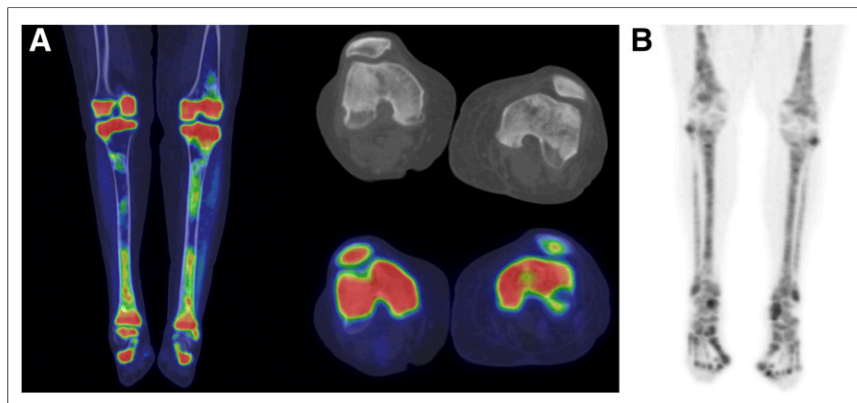


FIGURE 1. (A) ^{18}F -FDG PET/CT with coronal/axial fused and axial CT images of knees demonstrates predominantly patellar and epiphyseal ^{18}F -FDG-avid disease with associated sclerosis. (B) Maximum-intensity-projection PET image in different patient illustrates diffuse ^{18}F -FDG avidity involving small bones of feet.

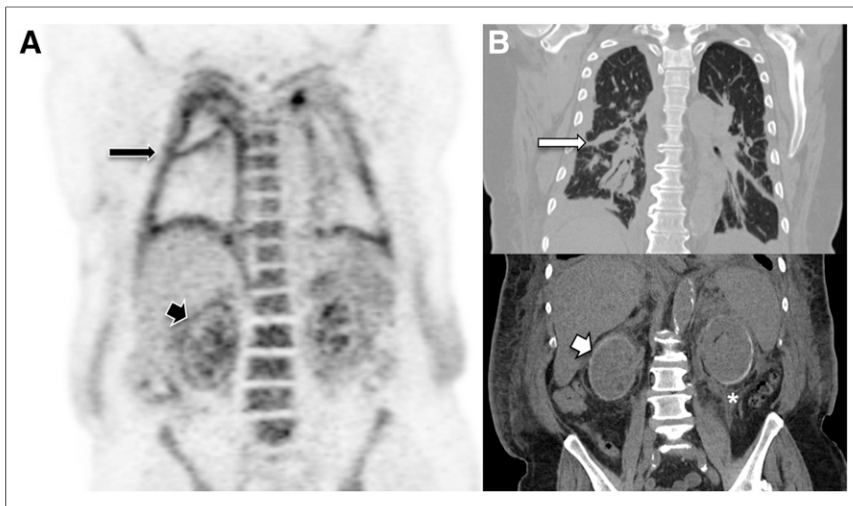


FIGURE 2. 71-y-old man with shortness of breath. (A) Coronal PET demonstrates increased pleural (long black arrow) and renal (short black arrow) ^{18}F -FDG activity. (B) Corresponding coronal CT depicts pleural thickening (long white arrow), bilateral perinephric fat stranding (hairy kidney) (*), and renal cortical calcification (goose egg kidney) (short white arrow).

47% of patients (15/32) had involvement of the axial skeleton and pelvis, including 6% of patients (2/32) with spinal involvement. Although appendicular long-bone disease was most frequently diaphyseal, epiphyseal involvement was also seen. One case showed greater epiphyseal and patellar involvement (Fig. 1A). Disease involving small bones of the feet was identified in 9% of patients (3/32) (Fig. 1B).

The kidneys were the second most common site of disease (81% [26/32]), with a mean SUV_{max} of 5.2 (range, 2.2–15.6). Renal disease was defined as increased ^{18}F -FDG avidity within the renal cortex or capsule. The CT component of ^{18}F -FDG PET/CT added confidence in identifying renal disease, with perinephric fat stranding (hairy kidney), poor corticomedullary differentiation (featureless kidney), and a rim of cortical calcification (“goose egg” kidney) (Fig. 2).

The CNS was the third most common site of disease (47% [15/32]), with a mean SUV_{max} of 10.7 (range, 3.8–34). CNS disease occurred throughout the neural axis and involved the cerebrum, cerebellum, pons, and spinal cord. Disease involving the spinal cord (12.5% [4/32]) and lumbosacral nerves (6% [2/32]) was evident only on

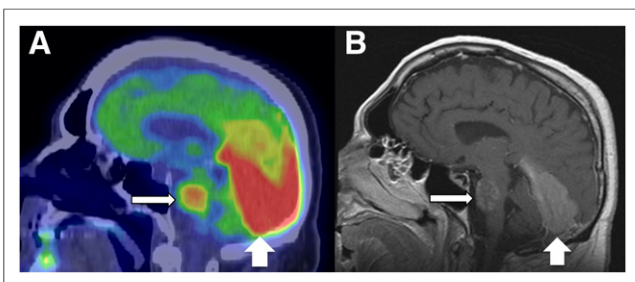


FIGURE 3. 50-y-old man with left mastoid pain. (A) Sagittal fused ^{18}F -FDG PET/CT demonstrates ^{18}F -FDG-avid disease within pons (thin white arrow) and along tentorium (thick white arrow). (B) Corresponding contrast-enhanced MRI illustrates infiltrative pons lesion (thin white arrow) and enhancing soft-tissue thickening along tentorium (thick white arrow).

the PET component of the examination. A solitary case of ^{18}F -FDG-avid suprasellar disease was identified. Extraaxial disease presented as thick plaque-like soft tissue, layered along dural membranes (Fig. 3). Suprasellar, filum terminale, and nerve root lesions were also identified.

Pulmonary parenchymal or pleural disease occurred in 41% of patients (13/32), with a mean SUV_{max} of 4.3 (range, 1.9–8.9). This finding predominantly involved the pleura and subpleural regions (Fig. 2). On CT, this presentation was most commonly manifested as smooth pleural and interlobular septal thickening.

Testicular hypermetabolism—some of which extended along the spermatic chord—was discovered in 40% of our male patients (8/20), with a mean SUV_{max} of 7.6 (range, 5.3–10.2). However, only 1 of these patients had associated scrotal symptoms.

Paranasal sinus disease was common (41% [13/32]), with an average SUV_{max} of 5.7 (range, 2.6–10). Most such disease occurred in the maxillary sinuses. The appearance of paranasal disease varied from mild mucosal ^{18}F -FDG avidity and a normal CT appearance to marked mucosal thickening, hypermetabolism, and osteoneogenesis.

Orbital disease occurred in 38% of patients (12/32), with a mean SUV_{max} of 5.4 (range, 3.0–10.9). CT changes ranged from subtle focal soft-tissue thickening to bulky bilateral intraconal soft tissue enveloping the optic nerve (Fig. 4). There were 2 cases of globe disease—1 with bilateral diffuse scleral thickening and low-level ^{18}F -FDG avidity and the other with marked bilateral chorioidal thickening and intense hypermetabolism.

Vascular disease—most commonly involving the aortic arch—occurred in 38% of patients (12/32), with an average SUV_{max} of 4.5 (range, 2.4–8.8). The heart and pericardium were involved in 34% of patients (11/32), with a mean SUV_{max} of 5.5 (range, 3.6–8.1).

Disease involving the retroperitoneal fascial planes, peritoneum, and central mesentery occurred in 34% of patients (11/32), with a mean SUV_{max} of 4.7 (range, 2.8–11.5). Lesions involving these sites appeared as plaque-like soft-tissue thickening. Mesenteric involvement had a perivascular predilection, commonly presenting as ^{18}F -FDG-avid soft tissue encasing the central vascular pedicle.

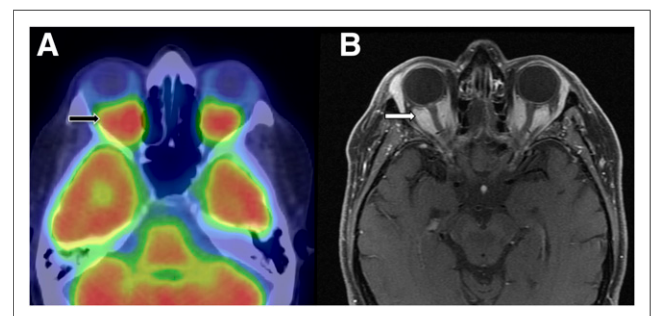


FIGURE 4. 59-y-old man with orbital pain. (A) Axial fused ^{18}F -FDG PET/CT demonstrates ^{18}F -FDG-avid soft tissue encasing intraconal spaces (arrow). (B) Corresponding axial T1-weighted fat-saturated contrast-enhanced MRI depicts enhancing intraconal soft tissue (arrow).

Two cases of female breast involvement presented as diffuse bilateral soft-tissue thickening and hypermetabolism. There were 2 cases of hepatobiliary disease—1 involving the hepatic parenchyma and the other tracking along the portal triad. We also discovered ECD involving the space of Retzius and the pancreas.

Only 2 patients had ^{18}F -FDG-avid lymph node disease, and these cases were isolated to regional nonenlarged lymph nodes with low-level hypermetabolism (SUV_{max} , 2.0–3.5). Neither was pathologically proven ECD. Both cases involved thoracic lymph nodes in the setting of active pulmonary ECD.

On the basis of PET Response Criteria in Solid Tumors methodology, 2 patients had a complete metabolic response—1 involving vemurafenib (BRAF+) and 1 involving anakinra (BRAF status unknown). Five patients had a partial metabolic response—3 involving vemurafenib (BRAF+), 1 involving pegylated interferon (peginterferon) (BRAF status unknown), and 1 involving prednisone (BRAF status unknown). Five patients had stable metabolic disease—1 involving vemurafenib (BRAF+), 2 involving peginterferon (BRAF-), and 2 involving cladribine (BRAF status unknown). One patient had progressive metabolic disease after peginterferon treatment (BRAF status unknown).

^{18}F -FDG PET/CT examination results affected patient management in 48% of cases (34/71). Eight examinations (11%) contributed to the initial diagnosis of ECD. Eight examinations (11%) supported a watchful waiting approach. Seven examinations (10%) contributed to the escalation of therapy. Five examinations (7%) directed biopsy. Two examinations (3%) supported continuation of therapy. One examination (1.4%) led to deescalation of therapy, whereas another examination (1.4%) ruled out a suspected pulmonary malignancy.

Significant correlations between ^{18}F -FDG PET/CT findings and BRAF+ status were identified. BRAF+ patients had higher mortality ($P = 0.0215$) and more frequent ^{18}F -FDG-avid CNS disease ($P = 0.0357$) than BRAF- patients. ^{18}F -FDG-avid CNS disease was able to predict the presence of a BRAF mutation with a sensitivity of 61%, a specificity of 88%, a positive predictive value of 92%, and a negative predictive value of 50%. No other correlations between BRAF+ status and pattern of disease were identified. However, patients with BRAF+ status had significantly higher SUV_{max} at their most metabolically active site of disease (9.7 [SD, 3.7]) than patients with BRAF- status (5.3 [SD, 2.2]) ($P = 0.0044$). The higher SUV_{max} of bone disease in BRAF+ patients also trended toward significance (4.5 [SD, 2.0] vs. 3.0 [SD, 1.3]; $P = 0.0914$).

There were no correlations between BRAF status and C-reactive protein level or erythrocyte sedimentation rate. However, patients with ^{18}F -FDG-avid mesenteric/peritoneal disease had higher C-reactive protein levels (55.2 [SD, 11.0] mg/L) than those without it (18.7 [SD, 8.2] mg/L) ($P = 0.0121$).

DISCUSSION

To our knowledge, we have reviewed the largest number of ^{18}F -FDG PET/CT examinations in a cohort of patients with histologically proven ECD. Correlations were discovered for BRAF+ status, intensity of ^{18}F -FDG-avid disease, and presence of CNS disease. About 50% of the ^{18}F -FDG PET/CT examinations affected patient management. A small number of examinations (10%) provided an initial benefit, either contributing to a diagnosis or guiding biopsy.

Most examinations (40%) affected management at follow-up, supporting prior reports highlighting the value of ^{18}F -FDG PET/CT in restaging (39). We observed increasing use of ^{18}F -FDG PET/CT for patients with ECD, perhaps indicating that referring physicians perceived a greater value of ^{18}F -FDG PET/CT.

Determining BRAF status in patients with ECD is an important branch of the clinical decision tree. Consensus guidelines recommend confirming negative BRAF results with more than 1 test modality or more than 1 sampled site (3). However, obtaining enough tissue for BRAF testing can be challenging, given tissue with a high ratio of fibrosis to histiocytes. Further, demineralization of bone samples impairs genetic analysis. Our data suggest that ^{18}F -FDG-avid CNS disease and higher SUV_{max} may act as biomarkers for BRAF positivity. Higher SUV_{max} has also been associated with BRAF+ status in papillary thyroid carcinoma, suggesting a common mechanism between BRAF mutations and hypermetabolism (43).

^{18}F -FDG PET/CT may be the most useful imaging modality for differentiating ECD from other histiocytoses. Given multiorgan involvement, ECD often elicits a broad differential diagnosis, including retroperitoneal fibrosis, IgG4-related disease, sarcoidosis, and other types of histiocytoses (44). A BRAF+ status essentially excludes other forms of non-Langerhans cell histiocytoses (45). Although lymph node involvement in ECD has been reported, it is rare (27,46,47). We confirmed this rarity, as only 2 patients (6%) in our cohort had mildly ^{18}F -FDG-avid lymph nodes, which may have been reactive given concomitant pulmonary disease. Moderate to high lymph node ^{18}F -FDG avidity (especially in more than 1 region) is therefore unlikely to be ECD related. In contrast, in Rosai-Dorfman disease, lymphadenopathy is a defining feature (48). ECD and LCH may involve the same organs. However, pulmonary disease and dermal disease are more characteristic of LCH, whereas cardiac involvement is a distinguishing feature of ECD (49). Along these lines, just over one-third (11/32) of our subjects had manifestations of ^{18}F -FDG-avid cardiac or pericardiac disease.

The disease distribution of ECD can be wide and difficult to predict. Our data support previous reports of disease involving nearly every organ system, including hepatobiliary, bowel, and large arteries (50–52). With a disease so varied, “unusual” may be the norm for ECD. Our data support the previous recommendation of a vertex-to-toe protocol in ^{18}F -FDG PET/CT scans for ECD patients (3).

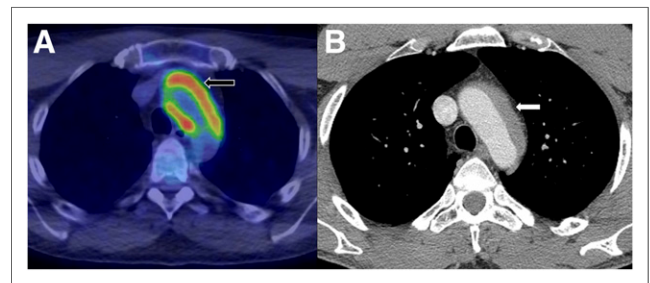


FIGURE 5. (A) Axial fused ^{18}F -FDG PET/CT of thorax demonstrates intensely ^{18}F -FDG-avid soft-tissue thickening surrounding aortic arch (arrow). (B) Corresponding contrast-enhanced CT demonstrates asymmetric soft tissue involving aortic arch in expected region of adventitia (arrow).

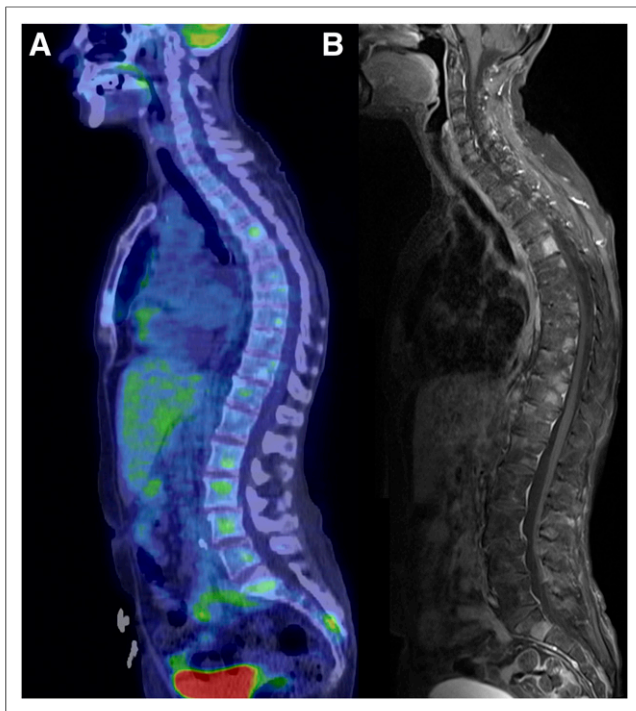


FIGURE 6. 63-y-old woman with back pain. (A) Fused sagittal PET/CT image of spine demonstrates multifocal ^{18}F -FDG-avid skeletal disease. (B) Contrast-enhanced fat-saturated T1-weighted sagittal MRI illustrates numerous enhancing lesions throughout spine.

Little information exists on ^{18}F -FDG PET/CT of CNS disease in ECD. Our findings support a prior report of intra- and extraaxial CNS involvement, including the cerebrum, cerebellum, brain stem, spinal cord, dura, and suprasellar space (21). Although MRI is likely more sensitive for detection and exact localization, our findings support a prior report demonstrating ^{18}F -FDG PET/CT utility in tracking the CNS ECD response to therapy (21).

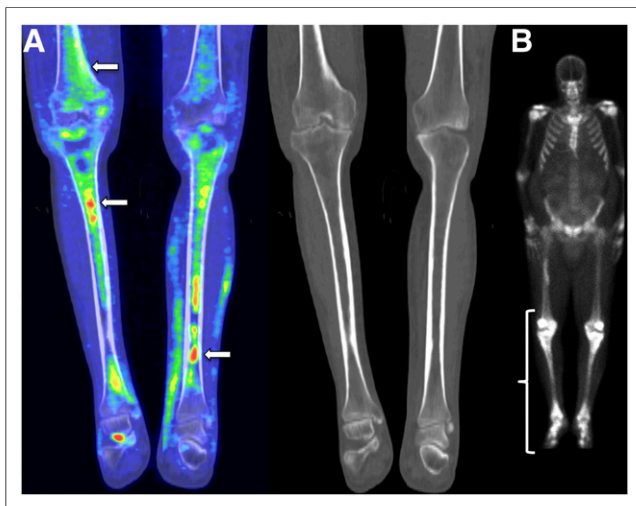


FIGURE 7. (A) Coronal ^{18}F -FDG PET/CT of distal lower extremities demonstrates ^{18}F -FDG-avid disease within both tibiae and distal femur (arrows) without osteosclerosis. (B) Anterior planar $^{99\text{m}}\text{Tc}$ -methylene diphosphonate whole-body bone scan demonstrates increased uptake throughout both distal lower extremities (bracket).

In the present study, the most characteristic vascular presentation was ^{18}F -FDG-avid soft tissue “coating” the aorta, corroborating a prior report of perivascular ECD involving the adventitial layer (Fig. 5) (53). We also found cardiac disease to have a right atrial propensity, similar to that previously reported (54).

Axial and pelvic skeletal involvement of ECD was once deemed rare (55). However, 47% of patients in our cohort (15/32) had axial or pelvic skeletal involvement, albeit generally less severe than appendicular disease (Fig. 6). The higher rate of axial disease in the present study may have been partly secondary to improvements in ^{18}F -FDG PET/CT technology. We also identified unique patterns of osseous ECD, with 9% of patients (3/32) showing involvement of the small bones of the feet and 1 patient showing predominantly epiphyseal/patellar disease. A prior report of an adolescent with ECD suggested that ^{18}F -FDG avidity may occur before radiographic evidence of sclerosis (56). Some cases from our cohort support this notion. However, we were unable to find a case of ^{18}F -FDG-avid osseous disease without a corresponding abnormal bone scan (Fig. 7).

The limitations of the present study included its retrospective nature and small sample size. Multiple methods were used to determine BRAF status; these methods had inherently different detection accuracies. Although many patients had received prior therapy, when we correlated ^{18}F -FDG PET/CT examinations with clinical data, we attempted to control for treatment effect by including only examinations from patients who had not received active treatment in the preceding 6 mo.

CONCLUSION

^{18}F -FDG PET/CT results may act as a biomarker for the presence of a BRAF mutation, aid in establishing a diagnosis, guide biopsies, and gauge the treatment response in ECD patients. Axial and pelvic skeletal involvement is greater than previously reported.

DISCLOSURE

No potential conflict of interest relevant to this article was reported.

REFERENCES

- Chester W. Über lipid Granulomatose. *Virchows Arch Pathol Anat.* 1930; 279:561–602.
- Emile JF, Abla O, Fraitag S, et al. Revised classification of histiocytoses and neoplasms of the macrophage-dendritic cell lineages. *Blood.* 2016;127:2672–2681.
- Diamond EL, Dagna L, Hyman DM, et al. Consensus guidelines for the diagnosis and clinical management of Erdheim-Chester disease. *Blood.* 2014;124:483–492.
- Blombery P, Wong SQ, Lade S, Prince HM. Erdheim-Chester disease harboring the BRAF V600E mutation. *J Clin Oncol.* 2012;30:e331–e332.
- Cangi MG, Biavasco R, Cavalli G, et al. BRAFV600E-mutation is invariably present and associated to oncogene-induced senescence in Erdheim-Chester disease. *Ann Rheum Dis.* 2015;74:1596–1602.
- Cui G, Liu D, Li W, et al. A meta-analysis of the association between BRAF mutation and nonsmall cell lung cancer. *Medicine (Baltimore).* 2017;96:e6552.
- Zhang Q, Liu SZ, Zhang Q, Guan YX, Chen QJ, Zhu QY. Meta-analyses of association between BRAF(V600E) mutation and clinicopathological features of papillary thyroid carcinoma. *Cell Physiol Biochem.* 2016;38:763–776.
- Løes IM, Immervoll H, Sorbye H, et al. Impact of KRAS, BRAF, PIK3CA, TP53 status and intraindividual mutation heterogeneity on outcome after liver resection for colorectal cancer metastases. *Int J Cancer.* 2016;139:647–656.
- Ding X, Zhang Z, Jiang T, et al. Clinicopathologic characteristics and outcomes of Chinese patients with non-small-cell lung cancer and BRAF mutation. *Cancer Med.* 2017;6:555–562.

10. Shain AH, Yeh I, Kovalyshyn I, et al. The genetic evolution of melanoma from precursor lesions. *N Engl J Med*. 2015;373:1926–1936.
11. Sosman JA, Kim KB, Schuchter L, et al. Survival in BRAF V600-mutant advanced melanoma treated with vemurafenib. *N Engl J Med*. 2012;366:707–714.
12. Swerdlow SH, Campo E, Pileri SA, et al. The 2016 revision of the World Health Organization classification of lymphoid neoplasms. *Blood*. 2016;127:2375–2390.
13. Haroche J, Charlotte F, Arnaud L, et al. High prevalence of BRAF V600E mutations in Erdheim-Chester disease but not in other non-Langerhans cell histiocytoses. *Blood*. 2012;120:2700–2703.
14. Goyal G, Shah MV, Call TG, Litzow MR, Hogan WJ, Go RS. Clinical and radiologic responses to cladribine for the treatment of Erdheim-Chester disease. *JAMA Oncol*. 2017;3:1253–1256.
15. Haroche J, Cohen-Aubart F, Emile JF, et al. Dramatic efficacy of vemurafenib in both multisystemic and refractory Erdheim-Chester disease and Langerhans cell histiocytosis harboring the BRAF V600E mutation. *Blood*. 2013;121:1495–1500.
16. Cohen-Aubart F, Emile JF, Maksud P, et al. Marked efficacy of vemurafenib in suprasellar Erdheim-Chester disease. *Neurology*. 2014;83:1294–1296.
17. Grumbine FL, Aderman C, Vagefi MR, Kersten RC. Orbital MRI pre- and post-vemurafenib therapy for Erdheim-Chester disease. *Ophthalm Plast Reconstr Surg*. 2015;31:e169.
18. Haroche J, Cohen-Aubart F, Emile JF, et al. Reproducible and sustained efficacy of targeted therapy with vemurafenib in patients with BRAF(V600E)-mutated Erdheim-Chester disease. *J Clin Oncol*. 2015;33:411–418.
19. Franconieri F, Martin-Silva N, de Boysson H, et al. Superior efficacy and tolerance of reduced doses of vemurafenib plus anakinra in Erdheim-Chester disease: towards the paradigm of combined targeting and immune therapies. *Acta Oncol*. 2016;55:930–932.
20. Gupta A, Yeganeh A, Rootman D, Goldberg R. Vemurafenib (BRAF inhibitor) therapy for orbital Erdheim-Chester disease. *Ophthalm Plast Reconstr Surg*. 2017;33:e138–e139.
21. Tzoulis C, Schwarzlmüller T, Gjerde IO, et al. Excellent response of intramedullary Erdheim-Chester disease to vemurafenib: a case report. *BMC Res Notes*. 2015;8:171.
22. Stempel JM, Bustamante Alvarez JG, Carpio AM, Mittal V, Dourado C. Erdheim-Chester disease, moving away from the orphan diseases: a case report. *Respir Med Case Rep*. 2016;20:55–58.
23. Haroche J, Arnaud L, Cohen-Aubart F, et al. Erdheim-Chester disease. *Curr Rheumatol Rep*. 2014;16:412.
24. Resnick D, Greenway G, Genant H, Brower A, Haghghi P, Emmett M. Erdheim-Chester disease. *Radiology*. 1982;142:289–295.
25. Waite RJ, Doherty PW, Liepman M, Woda B. Langerhans cell histiocytosis with the radiographic findings of Erdheim-Chester disease. *AJR*. 1988;150:869–871.
26. Dion E, Graef C, Miquel A, et al. Bone involvement in Erdheim-Chester disease: imaging findings including periostitis and partial epiphyseal involvement. *Radiology*. 2006;238:632–639.
27. Venkatanarasimha N, Garrido MC, Puckett M, White P. AJR teaching file: a rare multisystem disease with distinctive radiologic-pathologic findings. *AJR*. 2009;193:S49–S52.
28. Balink H, Hemmeler MH, de Graaf W, Grond J. Scintigraphic diagnosis of Erdheim-Chester disease. *J Clin Oncol*. 2011;29:e470–e472.
29. Wittenberg KH, Swensen SJ, Myers JL. Pulmonary involvement with Erdheim-Chester disease: radiographic and CT findings. *AJR*. 2000;174:1327–1331.
30. DeMartino E, Go RS, Vassallo R. Langerhans cell histiocytosis and other histiocytic diseases of the lung. *Clin Chest Med*. 2016;37:421–430.
31. Fortman BJ, Beall DP. Erdheim-Chester disease of the retroperitoneum: a rare cause of ureteral obstruction. *AJR*. 2001;176:1330–1331.
32. De Abreu MR, Chung CB, Biswal S, Haghghi P, Hesselink J, Resnick D. Erdheim-Chester disease: MR imaging, anatomic, and histopathologic correlation of orbital involvement. *AJNR*. 2004;25:627–630.
33. Loeffler AG, Memoli VA. Myocardial involvement in Erdheim-Chester disease. *Arch Pathol Lab Med*. 2004;128:682–685.
34. Haroche J, Amoura Z, Dion E, et al. Cardiovascular involvement, an overlooked feature of Erdheim-Chester disease: report of 6 new cases and a literature review. *Medicine (Baltimore)*. 2004;83:371–392.
35. Gauvrit JY, Oppenheim C, Girot M, et al. Images in cardiovascular medicine: high resolution images obtained with ultrasound and magnetic resonance imaging of pericarotid fibrosis in Erdheim-Chester disease. *Circulation*. 2004;110:e443–e444.
36. Adem C, Helie O, Leveque C, Taillia H, Cordoliani YS. Case 78: Erdheim-Chester disease with central nervous system involvement. *Radiology*. 2005;234:111–115.
37. Arnaud L, Pierre I, Beigelman-Aubry C, et al. Pulmonary involvement in Erdheim-Chester disease: a single-center study of thirty-four patients and a review of the literature. *Arthritis Rheum*. 2010;62:3504–3512.
38. Girszyn N, Arnaud L, Villain D, Kahn JE, Piette AM, Blety O. Usefulness of combined positron emission tomography and computed tomography imaging in Erdheim-Chester disease [in French]. *Rev Med Interne*. 2007;28:770–774.
39. Arnaud L, Malek Z, Archambaud F, et al. ¹⁸F-fluorodeoxyglucose-positron emission tomography scanning is more useful in followup than in the initial assessment of patients with Erdheim-Chester disease. *Arthritis Rheum*. 2009;60:3128–3138.
40. Antunes C, Graca B, Donato P. Thoracic, abdominal and musculoskeletal involvement in Erdheim-Chester disease: CT, MR and PET imaging findings. *Insights Imaging*. 2014;5:473–482.
41. Sioka C, Estrada-Veras J, Maric I, Gahl WA, Chen CC. FDG PET images in a patient with Erdheim-Chester disease. *Clin Nucl Med*. 2014;39:170–177.
42. Wahl RL, Jacene H, Kasamon Y, Lodge MA. From RECIST to PERCIST: evolving considerations for PET Response Criteria in Solid Tumors. *J Nucl Med*. 2009;50(suppl 1):122S–150S.
43. Lee SH, Han S, Lee HS, et al. Association between ¹⁸F-FDG avidity and the BRAF mutation in papillary thyroid carcinoma. *Nucl Med Mol Imaging*. 2016;50:38–45.
44. Caputo R, Marzano AV, Passoni E, Berti E. Unusual variants of non-Langerhans cell histiocytoses. *J Am Acad Dermatol*. 2007;57:1031–1045.
45. Cao XX, Sun J, Li J, et al. Evaluation of clinicopathologic characteristics and the BRAF V600E mutation in Erdheim-Chester disease among Chinese adults. *Ann Hematol*. 2016;95:745–750.
46. Lim J, Kim KH, Suh KJ, et al. A unique case of Erdheim-Chester disease with axial skeleton, lymph node, and bone marrow involvement. *Cancer Res Treat*. 2016;48:415–421.
47. Sheu SY, Wenzel RR, Kersting C, Merten R, Otterbach F, Schmid KW. Erdheim-Chester disease: case report with multisystemic manifestations including testes, thyroid, and lymph nodes, and a review of literature. *J Clin Pathol*. 2004;57:1225–1228.
48. Bösmüller H, Nann D, Horger M, Fend F. Erdheim-Chester disease and Rosai-Dorfman disease: pathological, radiological and clinical features of adult non-Langerhans cell histiocytosis [in German]. *Pathologe*. 2015;36:458–466.
49. Hervier B, Haroche J, Arnaud L, et al. Association of both Langerhans cell histiocytosis and Erdheim-Chester disease linked to the BRAFV600E mutation. *Blood*. 2014;124:1119–1126.
50. Pan A, Doyle T, Schlup M, Lubcke R, Schultz M. Unusual manifestation of Erdheim-Chester disease. *BMC Gastroenterol*. 2011;11:77.
51. Shah MV, Go RS. Erdheim-Chester disease. *Mayo Clin Proc*. 2015;90:1310.
52. Gundling F, Nerlich A, Heidland WU, Schepp W. Biliary manifestation of Erdheim-Chester disease mimicking Klatskin's carcinoma. *Am J Gastroenterol*. 2007;102:452–454.
53. Mazor RD, Manevich-Mazor M, Shoenfeld Y. Erdheim-Chester disease: a comprehensive review of the literature. *Orphanet J Rare Dis*. 2013;8:137.
54. Haroche J, Cluzel P, Toledano D, et al. Images in cardiovascular medicine: cardiac involvement in Erdheim-Chester disease—magnetic resonance and computed tomographic scan imaging in a monocentric series of 37 patients. *Circulation*. 2009;119:e597–e598.
55. Murray D, Marshall M, England E, Mander J, Chakera TM. Erdheim-Chester disease. *Clin Radiol*. 2001;56:481–484.
56. White TV, Silvester NC, Otero HJ. Non-sclerotic bone involvement in Erdheim-Chester: PET/CT and MRI findings in a 15-year-old boy. *Pediatr Radiol*. 2016;46:1345–1349.